ACS APPLIED MATERIALS & INTERFACES

Research Article

www.acsami.org

Biocompatibility of Soft-Templated Mesoporous Carbons

Maria F. Gencoglu,[†] Amanda Spurri,[‡] Mitchell Franko,[‡] Jihua Chen,[§] Dale K. Hensley,[§] Caryn L. Heldt,[†,*] and Dipendu Saha[‡,*]

[†]Department of Chemical Engineering, Michigan Technological University, 1400 Townsend Dr., Houghton, Michigan 49931, United States

[‡]Department of Chemical Engineering, Widener University, One University Place, Chester, Pennsylvania 19013, United States

[§]Center for Nanophase Materials Sciences, Oak Ridge National Laboratory, Oak Ridge, Tennessee 37831, United States

ABSTRACT: Soft-templated mesoporous carbon is morphologically a non-nano type of carbon. It is a relatively newer variety of biomaterial, which has already demonstrated its successful role in drug delivery applications. To investigate the toxicity and biocompatibility, we introduced three types of mesoporous carbons with varying synthesis conditions and pore textural properties. We compared the Brunauer–Emmett–Teller (BET) surface area and pore width and performed cytotoxicity experiments with HeLa cells, cell viability studies with fibroblast cells and hemocomapatibility studies. Cytotoxicity tests reveal that two of the carbons are not cytotoxic, with cell survival over 90%. The mesoporous carbon with the highest surface area showed slight toxicity (~70% cell survival) at the highest carbon concentration of 500 μg/mL. Fibroblast cell viability assays suggested high and constant viability of over 98% after 3 days with no apparent relation with materials property and good visible cell-carbon compatibility. No hemolysis (<1%) was confirmed for all the carbon materials. Protein adsorption experiments with bovine serum albumin (BSA) and fibrinogen revealed a lower protein binding capacity of 0.2–0.6 mg/m^2 and 2–4 mg/m^2 for BSA and fibrinogen, respectively, with lower binding associated with an increase in surface area. The results of this study confirm the biocompatibility of soft-templated mesoporous carbons.

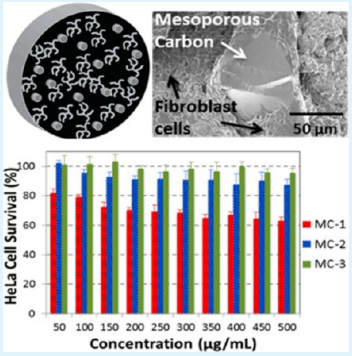

KEYWORDS: *mesoporous carbon, biocompatibility, cytotoxicity, cell viability, hemolysis, protein adsorption*

1. INTRODUCTION

Carbon-based materials have attracted great attention in biomedical and biological fields owing to their stability, chemical inertness, mechanical strength, and high surface area.[1] Morphologically, carbon-based materials can be classified into two distinct categories: nano carbons and non-nano carbons. Within the nano carbon variety, carbon nanotubes (CNTs) were considered to be an excellent material and examined several times for their characteristic biocompatibility.[2,3] Although the results from different research groups appeared to be conflicting and counterintuitive,[4] it has been almost universally accepted that CNTs are toxic, and their toxicity can be related to an adverse dermal,[5] respiratory,[6,7] pulmonary,[8,9] or cellular[10] response. It was also suggested that toxicity of CNTs varies widely with their degree of agglomeration, functionalization, and catalyst contents.[2−4] Besides CNTs, fullerenes also demonstrated characteristic toxicity.[11] On the other hand, non-nano carbons appeared to be much more benign. Diamond-like carbon (DLC) was employed as an attractive candidate for implant purposes, and it did not show significant toxic behavior.[12−14] Activated carbon is another type of non-nano carbon and has long been used for drug overdose and accidental toxin ingestion without any sign of toxicity.[15,16] Plenty of evidence has come to light that any nanosized particle may bear potential health hazards;[17] therefore, an approach toward building a non-nano carbon-based drug carrier might avoid any potential health risk in the first place.

Soft-templated mesoporous carbon is a relatively newer variety of synthetic, non-nano, and porous carbon that finds its key distinct features in controlled large pore accessibility and tunability of pore textures. Although mesoporous carbon has already established its role in the field of environmental applications, gas separation and storage, and energy harvesting, biological applications of this material are a relatively new and growing field. Synthesis of this material can employ different classes of amphiphilic surfactants for templating purposes, the role of which is very similar to that of silica in the case of hard-templating (i.e., to dictate mesoporosity). Typically, the cross-linked phenolic carbon precursors are held together by the micelles of amphiphilic surfactants through hydrogen bonding and translate the mesoporosity to the carbon matrix upon pyrolysis. Figure 1 shows the general schematic of fabricating an ideal mesoporous carbon from soft templates. Over time, both synthetic and natural carbon precursors were employed to fabricate mesoporous carbons by soft-templating. Recently published literature by part of our group and other researchers demonstrated that mesoporous carbon could be employed as a

Received: May 21, 2014
Accepted: August 21, 2014
Published: August 21, 2014

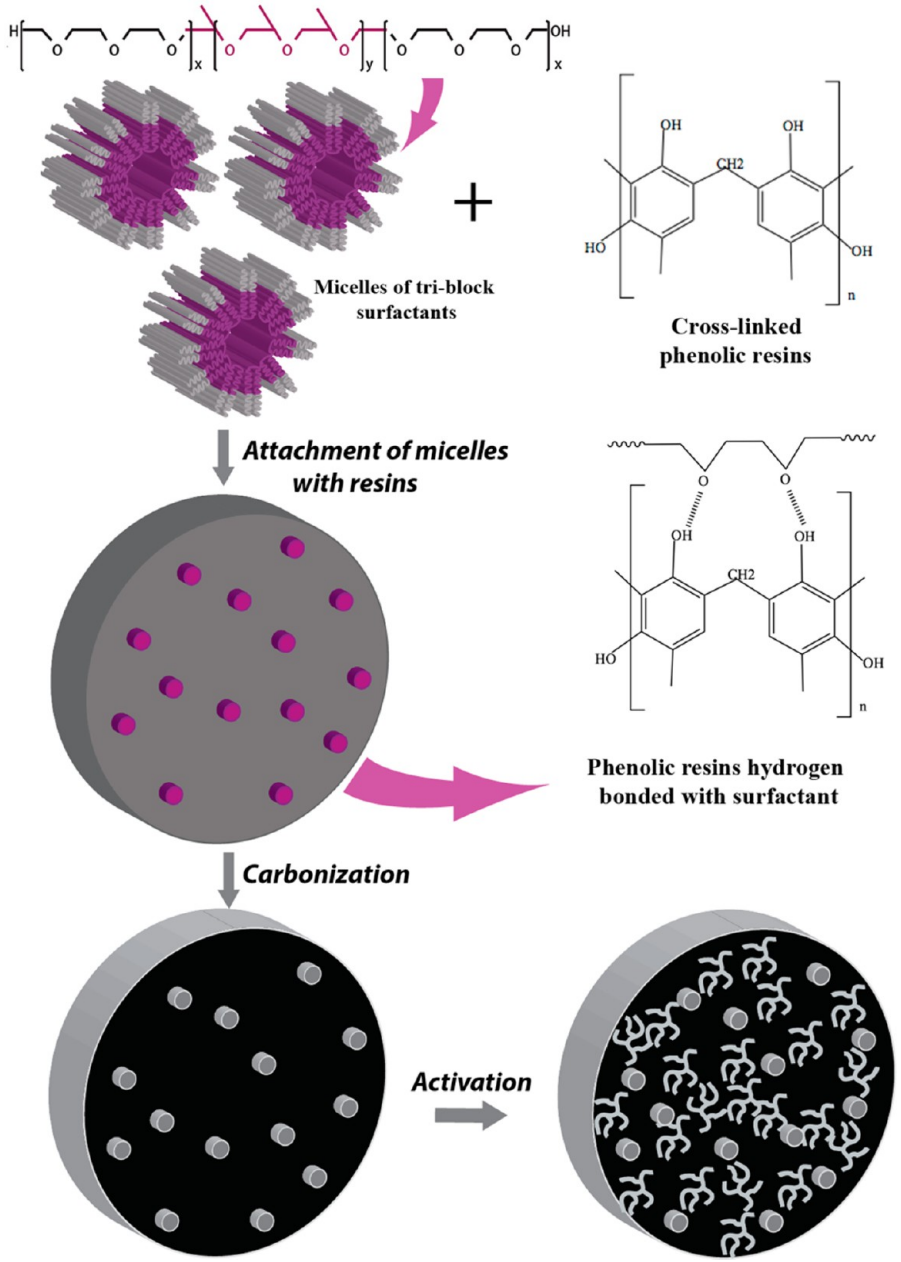

Figure 1. Generalized correlation of synthesizing an ideal mesoporous carbon from phenolic precursor via soft-templating. In this schematic, we have employed resorcinol-formaldehyde cross-linked resin as carbon precursor and a triblock copolymer, $[PEO]_x-[PPO]_y-[PEO]_z$ (PEO, poly(ethylene oxide); PPO, poly(propylene oxide)) as soft-template. For better visualization of micelles within phenolic resin and transformation of micellar regions onto mesopores, we have incorporated an imaginary circular sliced section of polymer composite and the resultant carbon upon carbonization and activation.

unique and controlled drug delivery vessel. Saha et al. reported successful controlled release of four model drugs—captopril,[18,19] ranitidine hydrochloride,[19] furosemide,[19] and antipyrine[20] from mesoporous carbons—aimed toward oral drug delivery. Ibuprofen,[21,22] indomethacin,[22] and lovastatin[23] were three other drugs that were employed to examine the performance of mesoporous carbon as drug delivery vehicles. Besides oral drug delivery, nanosized or thin film of mesoporous carbons were also successfully employed for controlled and targeted release of anticancer drugs, namely, doxorubicin,[24] camptothecin,[25] and mitoxantrone,[26] aimed toward blood plasma or transmembrane delivery.

Owing to the disadvantages of mesoporous silica or metal–organic frameworks (MOFs) as drug delivery vehicles,[19,27−31] mesoporous carbon could be a better choice as a porous-media-based drug delivery system, in addition to its high material tunability. Although there are several reports on mesoporous carbons as drug delivery vehicles, biocompatibility studies of this material are quite handful and not universal. Karavasili et al.[22] performed toxicity and cellular uptake studies of mesoporous carbons with human colon carcinoma (Caco-2) cells that revealed no significant toxicity or abnormal change in cell morphology in contact with mesoporous carbons. Zhao et al.[23] examined the cytotoxicity of uniform mesoporous carbon spheres with the same type of cells (Caco-2) and revealed no

cytotoxicity. Zhu et al.[24] and Kim et al.[32] confirmed the null toxicity of nanosized mesoporous carbon particles on cervical cancer (HeLa) cells. Fang et al.[33] reported similar evidence of zero toxicity of mesoporous carbons with human nasopharyngeal epidermoid carcinoma (KB) cells. Gu et al.[25] reported on the in vitro cytotoxic behavior of camptothecin loaded mesoporous carbon, but they did not report the toxicity studies of pristine carbons. Although the past literature confirmed zero to minimal cytotoxicity of mesoporous carbons, these studies did not verify other parameters of biocompatibility, including the role of pore textural properties on the degree of biocompatibility.

In this collaborative research, we have synthesized soft-templated mesoporous carbon from two phenolic precursors, resorcinol and phloroglucinol, and two triblock copolymers, Pluronic F127 and 17R4, as soft templates along with post-synthesis activation to improve the pore textural properties. We have incorporated these materials with varying porosity in the studies of cell toxicity with HeLa cells, cell growth with fibroblast cells, blood protein adhesion, and hemolysis. To the best of our knowledge, this is the first report on the detailed biocompatibility studies of mesoporous carbons or any nanoporous carbon, in general. The mesoporous carbons were fabricated by using varying synthesis conditions and contain different degrees of porosity so that the results of the study can be analyzed and interpreted in a broad platform.

2. EXPERIMENTAL PROCEDURES

2.1. Materials Synthesis. First, 50 g of resorcinol and 40 g of Pluronic F127 were dissolved in a mixture of 400 mL of water/20 mL of ethanol with 60 mL of HCl (6 M) for 1 h 30 min. After that, 48 mL of formaldehyde as a cross-linking agent was added and stirred for 2 h until the polymer layer settled to the bottom with the solvent on top. The polymer layer was separated and carbonized in a tube furnace in a N_2 flow from room temperature to 400 °C at a rate of 1 °C/min, and from 400 to 1000 °C at a rate of 2 °C/min; the final temperature was maintained for 15 min, followed by cooling to room temperature in the same N_2 flow. To perform the activation, we mixed this material with solid KOH in a 1:3 ratio, heated the mixture in the tube furnace in a N_2 flow from room temperature to 1000 °C at a rate of 10 °C/min, and cooled the mixture in the same N_2 flow. The activated and inactivated materials are termed as MC-1 and MC-2, respectively. To synthesize another material, we mixed 100 g of phloroglucinol and 140 g of Pluronic 17R4 in a mixture of 320 mL of water/480 mL of ethanol in the presence of 60 mL of HCl (6 M), followed by addition of 96 mL of formaldehyde. The polymer was collected in a similar fashion and carbonized with the same protocol. This material was named MC-3.

2.2. Materials Characterization. MC-1, MC-2, and MC-3 were characterized with pore textural properties in a Quantachrome Autosorb iQ (Boynton Beach, FL) by N_2 adsorption−desorption at liquid N_2 temperature (77 K) and CO_2 adsorption−desorption at 273 K. Brunauer−Emmett−Teller (BET) specific surface area and pore size distribution by nonlocal density functional theory (NLDFT) were calculated by using the instrument's built-in software. High-resolution transmission electron microscopic (TEM) images were obtained in a Carl Zeiss Libra 120 TEM (Thornwood, NY) operating at 120 kV. The samples were dispersed in ethanol at about 0.5 wt % concentration and ultrasonicated for 5 min before being drop-casted onto an amorphous carbon (~20 nm in thickness) coated TEM grid (Ted Pella). Scanning electron microscope (SEM) images of pure mesoporous carbons samples were obtained in a Carl Zeiss Merlin SEM operating at 30 kV. No additional sample preparation protocol was employed for SEM images; the as-received samples were directly inserted into the sample holder for image capturing. The energy-dispersive X-ray spectroscopy (EDXS) results were obtained with a system from Bruker Nano GmbH using an XFlash detector 5030. The analysis was conducted with Bruker's Quantax Esprit Hypermap mode. The elements were selected using the automatic and find modes. Once a map was obtained, a 25 μm area of interest was selected for the map data results so an average could be obtained. The interactive standards were set during the quantify method. The SEM high voltage was set to 30 kV, and the stage was tilted 30° to help alleviate the problem of absorption of X-rays by the rough surface. Sample thickness varied from 10 to 100 μm. The SEM stage holder and tweezers were cleaned with isopropyl alcohol and clean wipes. Fresh carbon tape was employed to mount the samples.

2.3. Cytotoxicity. HeLa cells (H1HeLa, CRL1958) were purchased from ATCC (Manassas, VA) and propagated in HeLa media, which consisted of minimum essential medium (MEM) (Life Technologies, Carlsbad, CA) supplemented with 5% fetal bovine serum (FBS) (Atlanta Biologicals, Norcross, GA) and 1% penicillin/streptomycin (pen/strep) (Life Technologies, Carlsbad, CA). The cells were propagated at 37 °C, 5% CO_2, and 100% humidity. HeLa cells were seeded in a 96-well plate at a density of 8×10^4 cell/ml and 100 μL of cells per well. Stock solutions were prepared with 500 μg/mL of mesoporous carbon samples in HeLa media and sonicated for 20 min in a Misonix XL-2000 Ultrasonic Probe Sonicator (Sonics & Materials, Inc., Newtown, CT). Samples ranging from 50 to 450 μg/mL were prepared from the stock solution. All the samples, including the stocks were sonicated in an Ultrasonic Water Bath (VWR, West Chester, PA) for 20 min. Samples were added to the cells after 24 h at a volume of 25 μL. Cell activity was measured after 5 days by the conversion of the MTT tetrazolium salt (3-(4,5-dimethylthiazol-2-yl)-2,5-diphenyl tetrazolium bromide; VWR, Radnor, PA) to its formazan form and was performed according to previous studies.[34] Percent survival was calculated with eq 1:

$$\%\ \text{survival} = \left(\frac{A_{\text{mc}}}{A_{\text{mock}}}\right) \times 100 \tag{1}$$

where A_{mc} and A_{mock} are the absorbance of the mesoporous carbon (mc) and the mock media (mock), respectively.

2.4. Cell Viability. Fibroblast (NIH/3T3, CRL1658), purchased from ATCC were propagated in fibroblast media, which consisted of Dulbecco's modified Eagle medium (DMEM) (Life Technologies, Carlsbad, CA) supplemented with 5% FBS and 1% pen/strep. Fibroblast cells were grown at 37 °C, 5% CO_2, and 100% humidity. Mesoporous carbon samples at 100 μg/mL in fibroblast media were sonicated for 20 min in a Misonix XL-2000 Ultrasonic Probe Sonicator. Samples were added to 24-well plates at a volume of 100 μL/well. After the samples were added, fibroblast cells were seeded on the mesoporous carbon samples at a density of 2.5×10^5 cells/ml and 500 μL per well. Cells were incubated with the mesoporous carbon samples for 1−4 days. Cell viability was measured with a trypan blue exclusion assay. After the media were removed, 200 μL of 0.25% trypsin/ethylenediaminetetraacetic acid (EDTA; Life Technologies, Carlsbad, CA) was added to detach cells from the well and the mesoporous carbon. Then, 200 μL of fibroblast medium was added to inactivate the trypsin. Next, 40 μL of trypan blue stain (0.4%) (Life Technologies, Carlsbad, CA) was added to the cells, and the viable and nonviable cells were counted in a hemocytometer. Trypan blue was excluded from cells with an intact cell membrane, and these cells are assumed to be viable. Percent viability was calculated with eq 2:

$$\%\ \text{viability} = \left[1 - \left(\frac{N_{\text{dc}}}{N_{\text{tc}}}\right)\right] \times 100 \tag{2}$$

where N_{dc} and N_{tc} are the number of dyed cells (dc) and total cells (tc), respectively.

2.5. Hemolysis Test. Human blood samples for the hemolysis test were obtained from a voluntary donor at the Portage Health Clinic at Michigan Technological University. All work was performed in a certified Biosafety Level 2 laboratory with approval from the Internal Review Board (IRB). The hemolysis test was conducted as stated by Fan et al.[35] Briefly, the blood sample was collected in tubes containing EDTA and diluted 10-fold in a saline solution (0.9% NaCl). The diluted blood was centrifuged at 1500 rpm for 10 min in an Accu Spin

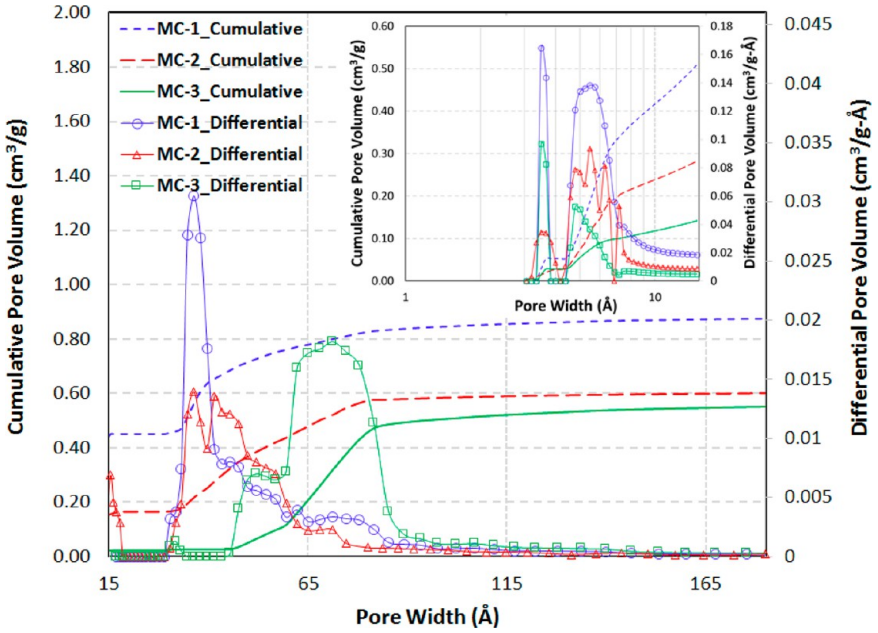

Figure 2. Pore size distributions of MC-1, MC-2, and MC-3. (Inset) Micropore distribution of the mesoporous carbon samples calculated from CO_2 adsorption isotherm at 273 K; pore width is in log scale.

400 centrifuge (Thermo Fisher Scientific, Waltham, MA). The upper phase was removed, and the packed erythrocytes were washed three times with saline solution. Packed erythrocytes were diluted 2 v/v % in saline solution. Stock mesoporous carbon samples of 500 μg/mL were prepared in saline solution and sonicated for 20 min in a Misonix XL-2000 Ultrasonic Probe Sonicator. Four samples ranging from 100 to 500 μg/mL were prepared from the stock solution and sonicated in an ultrasonic water bath for 20 min. After sonication, 0.45 mL of diluted erythrocytes were added to 0.45 mL of carbon sample and equilibrated at 37 °C. Diluted erythrocytes were also added to NanoPure water (Thermo Scientific, Waltham, MA; resistance >18 MΩ; positive control) and to saline solution (negative control). After 1 h, samples were centrifuged at 1500 rpm for 10 min. The supernatant was removed and the absorbance was measured on a Synergy Mx microplate reader (BioTek, Winooski, VT) at 545 nm. Percent hemolysis was calculated with eq 3:

$$\%\ \text{hemolysis} = \left(\frac{A_{mc} - A_{neg}}{A_{pos} - A_{mc}}\right) \times 100 \quad (3)$$

where A_{mc}, A_{neg}, A_{pos}, were the absorbance of the mesoporous carbon (mc), the negative control (neg), and the positive control (pos), respectively.

2.6. Protein Adsorption. Albumin from bovine serum (BSA) and fibrinogen from bovine plasma, purchased from Sigma-Aldrich, (St. Louis, MO), was diluted in phosphate-buffered saline (PBS, pH 7.2) (Life Technologies, Carlsbad, CA) to a final concentration of 1 mg/mL. The protein solutions were incubated with 0.0025 g of mesoporous carbon samples for 2 h at 37 °C. Protein absorbance before and after contact with mesoporous carbon samples was measured on a Synergy Mx microplate reader at 280 nm. The difference between the concentrations before and after incubation with the carbon samples was determined as the concentration adsorbed on the mesoporous carbon samples.

2.7. Imaging of Cell Growth on Mesoporous Carbon Materials. Cell growth on mesoporous carbon samples was done in a way similar to that of Correa-Duarte et al.[36] Fibroblast cells were seeded on mesoporous carbon samples, as described in section 2.4. After 3 days, the cells attached to mesoporous carbon samples were scrapped out of the plates and placed into centrifuge tubes. Samples were centrifuged at 1500 rpm for 10 min in a Sorvall ST16R Centrifuge (Thermo Fisher Scientific, Waltham, MA) and washed 3 times with 500 μL of PBS. Samples were fixed with 500 μL of 2.5% glutardehyde (Sigma-Aldrich, St. Louis, MO) in 0.1 M sodium cacodylate (Sigma-Aldrich, St. Louis, MO), pH 7.4, for 2 h at 4 °C. After several washes with 0.1 M sodium cacodylate, samples were dehydrated with ethyl alcohol (Pharmco-Aaper, Brookfield, CT) in series (25%, 50%, 75%, 95%, 100%, 100%) for 10 min at each step. Samples were chemically dried in 1,1,1,3,3,3-hexamethyldisilazane (HMDS) (Thermo Fisher Scientific, Waltham, MA) in series at 50% and 100% for 10 min at each step and placed overnight in a fume hood at 22 °C. Samples were mounted and coated with 2.5 nm of platinum/palladium (Hummer Sputtering System, Union City, CA) and imaged with a Hitachi S-4700 cold-field emission scanning electron microscope (FE-SEM; Tustin, CA) with an accelerating voltage of 5 kV.

3. RESULTS AND DISCUSSIONS

3.1. Materials Characterization. The BET specific surface area (SSA) of MC-1 and MC-2 are 1221 and 560 m^2/g, respectively. MC-3 represents the lowest BET surface area of 315 m^2/g. Pore size distributions of these three materials calculated by NLDFT are shown in Figure 2. The pore textural characteristics, including BET SSA, external SSA, and total pore volume are provided in Table 1. MC-1 and MC-3 possess the median mesopore width of 36 and 70 Å with a total pore volume of around 0.9 and 0.55 mL/g, respectively. To visualize the presence of micropore distributions present in these samples, we employed CO_2 adsorption isotherms, and the pore size distribution plot is inserted as an inset in Figure 2.

Table 1. Pore Textural Properties of Mesoporous Carbons Samples

carbon species	BET SSA (m^2/g)	external SSA (m^2/g)[a]	total pore volume (mL/g)[b]
MC-1	1221	399	0.90
MC-2	560	322	0.60
MC-3	315	244	0.55

[a]Calculated by statistical thickness (*t*-plot) method. [b]Calculated by NLDFT method.

MC-3 shows a higher mesopore width at 70 Å with a lower mesopore volume of 0.55 mL/g. TEM images (Figure 3a,c,e) of

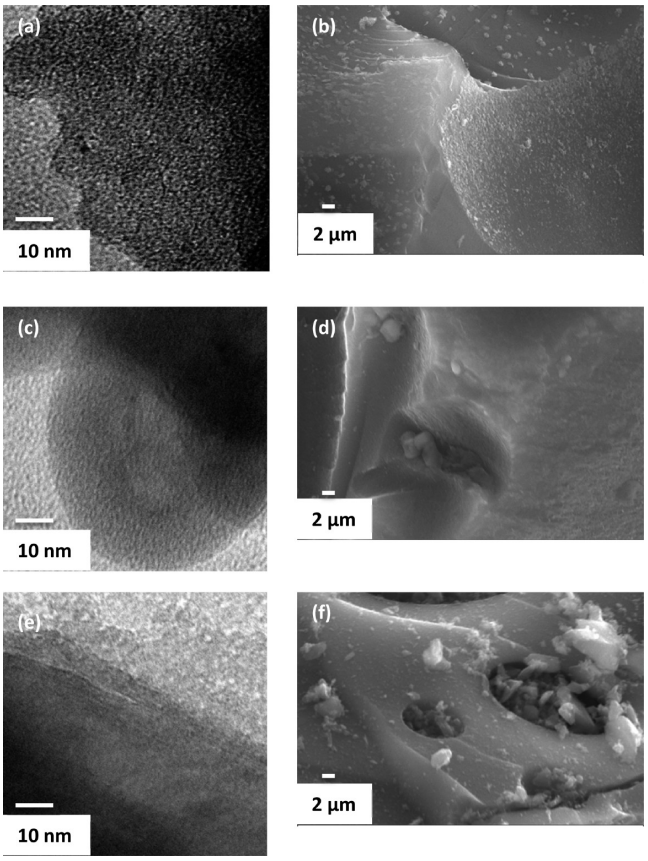

Figure 3. Electron microscopic images of mesoporous carbon samples. (a) TEM and (b) SEM images of MC-1; (c) TEM and (d) SEM images of MC-2; (e) TEM and (f) SEM images of MC-3.

these mesoporous carbons did not reveal a geometrical order of pores; instead, it demonstrated a "worm-like" porous entity in the carbon matrix. SEM images (Figure 3b,d,f) showed that all the mesoporous carbon particles are highly irregular in external morphology. We performed EDXS studies to get the elemental analysis of the carbon samples, and the results are shown in Table 2. The carbon content varies within 80−87% along with

Table 2. Elemental Analysis of Mesoporous Carbons Samples

carbon species	carbon (%)	oxygen (%)	potassium (%)	others (%)
MC-1	87.06	12.04	0.76	0.14
MC-2	79.59	19.77	0.03	0.61
MC-3	80.76	18.76	0.01	0.47

a large proportion of oxygen, 12−19%. The origin of oxygen can be rooted to the hydroxyl groups in the carbon precursors that might have converted to other carbon containing functional groups during chemical reaction and carbonization. Slightly lower oxygen content in MC-1 can most likely be attributed to the reheating of the carbon sample during activation, which might have caused cleavage of oxygen-containing functional groups. Presence of oxygen in metallic oxides, possibly arrived from porcelain boats in the course of carbonization, may also contribute to total oxygen content, although such contribution is much smaller compared to the surface functionality. MC-1 also has a higher percentage of potassium (0.76%) compared to the rest of the carbon samples, and that can definitely be attributed to the activation with KOH. All the mesoporous carbon samples contain a very small fraction of nitrogen and trace elements (0.14−0.47% aluminum, zirconium, calcium, and magnesium) that might have originated from the porcelain boat in the course of carbonization or from an impurity in the precursor chemicals.

3.2. In Vitro Cell Interactions. In vitro biocompability and toxicity tests are the prerequisites for any biomaterials prior to in vivo animal model evaluation and clinical trials.[2,12] Mesoporous carbon toxicity was examined in HeLa cells with an MTT cell viability assay. The MTT assay is a common method employed to measure the biochemical activity of cells seeded on carbon materials.[37,38] Figure 4 shows the results of

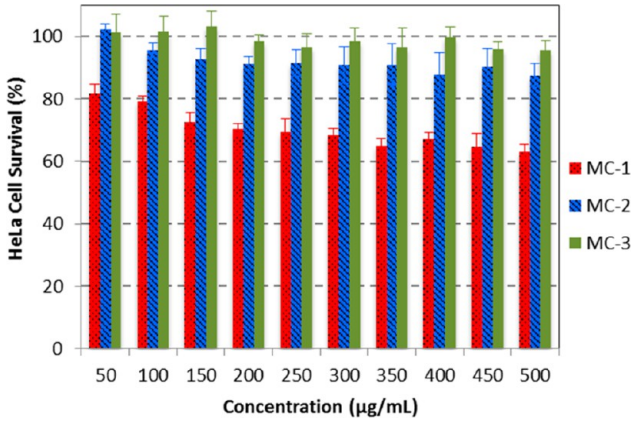

Figure 4. Cytotoxicity of mesoporous carbon samples in HeLa cells. Cells were incubated with mesoporous carbon materials for 5 days, followed by evaluation of cell viability with an MTT Assay. Percent survival is defined in eq 1. All data points are the average of three separate experiments; error bars represent the standard deviation.

cytotoxicity studies of the mesoporous carbons; none of the carbon samples demonstrated acute cytotoxicity. MC-2 and MC-3 demonstrated negligible toxicity in the range of 50−500 μg/mL (survival > 90%). MC-1 showed slight toxicity with cell survival decreasing with an increase in concentration and demonstrated around 70% survival at the highest concentration tested (500 μg/mL). The concentration-dependent cell survival of the mesoporous carbon materials are higher than the nanosized mesoporous carbon reported by Fang et al.[33] in which cell survival was not more than 60% at a much lower carbon concentration of 100 μg/mL with a shorter incubation period of 24 h. A closer inspection of our results can reveal a definite pattern of cytotoxicity, that is, it increases with the increase in surface area of the carbon materials tested (MC-3 < MC-2 < MC-1) at all concentrations. In fact, such dependence of cytotoxicity is quite prevalent not only in the case of porous carbon materials,[23] but also for mesoporous silicas.[39,40]

The so-called cytotoxicity at the higher carbon concentration may be attributed to the simple reason for physical hindrance to the cell proliferation;[22] however, the patterned toxicity may need different explanations. Unlike nanosized carbons, the cellular uptake of the carbon matrix can definitely be ruled out for any of our samples. Although external morphologies, including shapes and size of porous matrix, were counted as plausible credentials for porous silica toward cytoxocity,[39] the

mesoporous carbon samples tested in this study are highly irregular in shape and, most likely, a shape factor did not contribute toward toxicity. A closer inspection suggests the size of MC-1 and MC-2 are in the order of 20−50 μm in size, whereas MC-3 particles are larger than 100 μm. Smaller particles may interact better with the HeLa cell (size, ∼14 μm), providing a stronger obstruction toward their proliferation. It is also noteworthy that the external surface areas are also in the exact order of cytotoxicity (MC-3 < MC-2 < MC-1), and the greater external surface area also possesses a greater chance of more intimate interactions with cellular bodies.

Surface chemistry is another significant factor that may corroborate the patterned toxicity. Although MC-1 has a higher concentration of potassium, the literature does not provide any evidence that potassium causes cytotoxicity. MC-1 has the lowest concentration of oxygen (Table 2), which essentially means it has lower percent of oxygen-containing functional groups and possesses the highest carbon content. As the oxygen-containing functional groups may have greater chance for providing higher degree of hydrophilicity on the hydrophobic carbon surface, MC-1 could be more hydrophobic than rest of the samples. It is mentioned in the literature[41] that a hydrophilic surface can interact with a protein surface through an intermediate layer of water molecules, whereas a hydrophobic surface possesses a higher chance of directly interacting with such proteins. This direct interaction could cause denaturation and conformational changes of the proteins. One known effect of hydrophobic surface interaction with cells has been shown to lead to the adverse effects of adenosine triphosphate (ATP) depletion and triggering of cell apoptosis.[42] It is also suggested that a hydrophobic surface itself may provide a higher risk of cell apoptosis.[43] Although the higher toxicity of MC-1 can be attributed to its hydrophobic nature, such interactions may not be supportive to distinguish the cytotoxic behavior between MC-2 and MC-3, as both of them possess similar oxygen content and apparently the same hydrophobic/hydrophilic nature.

Earlier it was suggested that a material with high external surface area would be less favorable as a biomaterial owing to its higher cytotoxicity.[44] Our results demonstrated that the internal or BET surface area could be the most intriguing factor toward explaining the cytotoxicity pattern. Earlier, it was reported that silica could be responsible for generating the reactive oxygen species (ROS) radicals that cause cell damage.[45] Yet, the precise role of surface area as a catalytic agent in such phenomena was neither properly understood nor thoroughly investigated. We hypothesize that another indirect phenomena may also be responsible for this effect. We suggest that a higher surface area material can inherently adsorb larger amount of nutrients within its porous moiety from the proximity of or in contact with the cellular bodies, and therefore, the cells may die because of lack of nutrients to survive. Such phenomena, if true, can support the patterned cytotoxic behavior. However, more rigorous experiments with varying conditions, which are not within the scope of this work, are required to experimentally validate this hypothesis. Nevertheless, the overall experimental work suggests that mesoporous carbon samples demonstrated minimal cytotoxic nature and are benign, similar to other non-nano carbons.[46]

To investigate cell viability, we incubated the mesoporous carbon samples with fibroblast cells from 1 to 4 days, along from the mock media as a control substrate for comparison. The concentration of carbon samples employed was 100 μg/mL. The results of this study indicate that cell viability was very high and almost constant (>98%) from day 1 to day 3 without any significant difference with the mock media (Figure 5a).

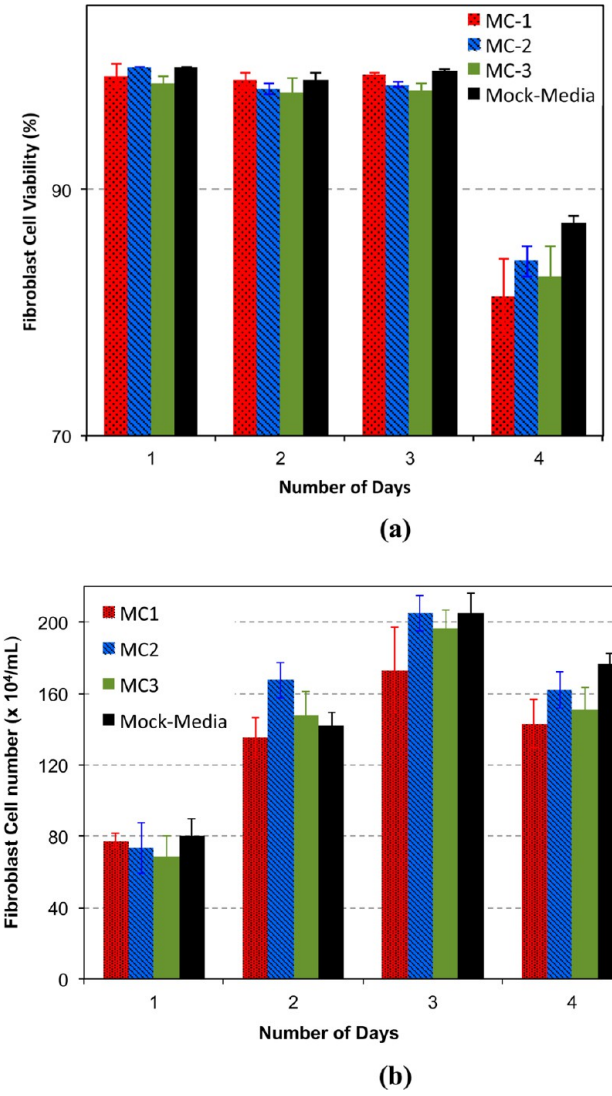

Figure 5. Biocompatibility of mesoporous carbon samples in fibroblast cells. (a) Percent viability and (b) cell number. Cells were incubated with mesoporous carbon materials from 1 to 4 days. Cell viability was measured with a trypan blue exclusion assay. Percent viability is defined in eq 2. All data points are the average of three separate experiments; error bars represent the standard deviation.

After the third day, cell viability decreased (∼82%) for all the mesoporous carbon samples tested, including the mock media. The number of fibroblast cells also decreased after the third day for all the samples and the mock media (Figure 5b). The cause of the decreasing trend in cell populations can certainly be ascribed to the lack of nutrients in the culture medium without any possible influence of the mesoporous carbons. The cells likely needed fresh media with nutrients after the third day of culture, but it was not possible to replenish them with fresh nutrients in the course of experiments owing to the atypical nature of dispersed mesoporous carbons in culture media. It is also noteworthy to mention that the cell viability assay did not reveal a patterned behavior with mesoporous carbons, and it

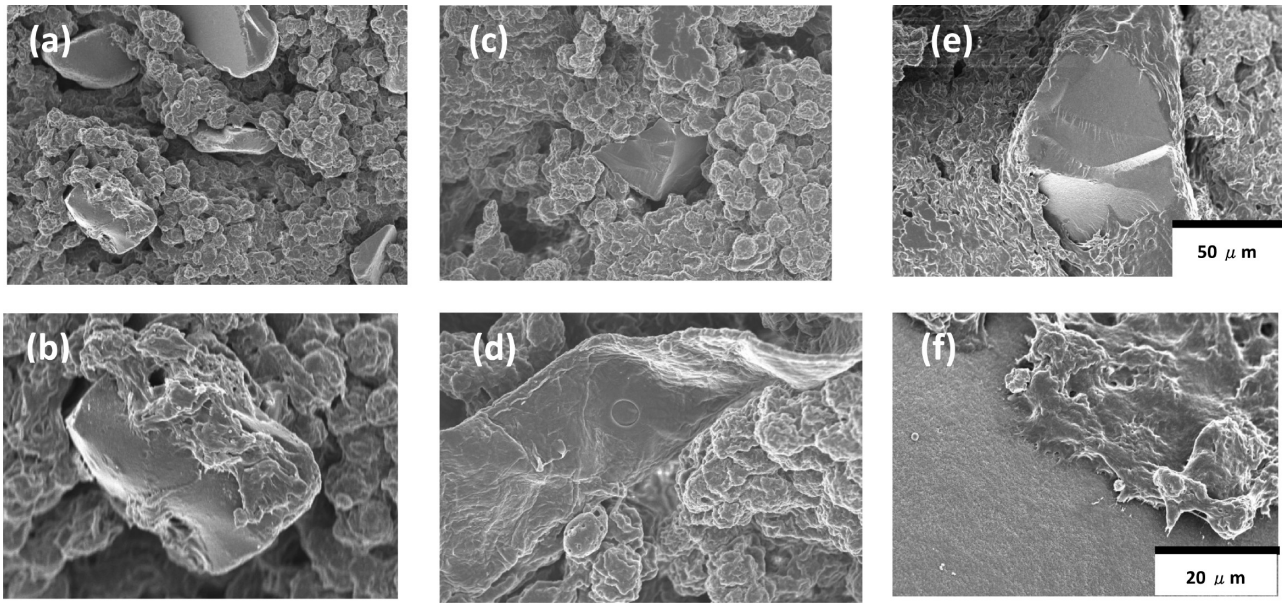

Figure 6. Fibroblast cell growth on mesoporous carbon samples. (a and b) MC-1, (c and d) MC-2, and (e and f) MC-3. Cells were incubated with carbon samples for 3 days. Scale bars are (top) 50 and (bottom) 20 μm.

essentially confirms that cell viability is independent of porosity, size, and shape of such materials.

We have analyzed the growth of fibroblast cells on mesoporous carbon samples with FE-SEM for visual inspection purposes (Figure 6). All the mesoporous carbon samples were incubated with fibroblast cells for 3 days. We found that the fibroblast cells surrounded the carbon particles, suggesting that the carbon surface did not offer adverse effects to the proliferation of cells. Although all three varieties of carbon provided good platforms for fibroblast cell growth, MC-3 appeared to demonstrate a better contact and adhesion surface for the cells, as shown in Figures 6e,f. Apparently, better cell compatibility of MC-3 is in agreement with its highest cell survival with HeLa cells, but it did not provide a similar trend with fibroblast cell viability and cell number (Figure 5a,b), suggesting that cell contact has a minimal influence in the viability assay. The better adhesion properties of MC-3 may be attributed to the lower porosity of the material, providing better "anchoring", higher hydrophilic surface, or better transport of nutrients through the larger pores of the MC-3 material.

3.3. Hemocomapatibility of Mesoporous Carbon Materials. The hemocomapatibility of a drug carrier is the prerequisite for intravascular drug delivery. In our study, we employed two hemocomapatibility tests: hemolysis and adsorption of blood plasma proteins. Hemolysis studies determine the stability of red blood cell (RBC) in contact with a foreign body. Four concentrations of mesoporous carbons ranging from 100 to 500 μg/mL were employed to examine the hemolysis. The results are shown in Table 3.

Primary observations suggest that the hemolysis is minimum (< 1%) for all samples at all concentrations. Although the majority of the data represented demonstrated slight enhancement of hemolysis with an increase in carbon concentration from 100 to 500 μg/mL, we did not find ubiquity of such behavior. Additionally, the relationship of hemolysis with different samples (i.e., surface area and particle size) did not reveal any patterned behavior. Such behavior is in complete disagreement with previous studies with mesoporous and nanosized silica particle, where hemolysis was proved to be a

Table 3. Hemolysis (%) Caused by Mesoporous Carbon Samples[a]

carbon species	100 μg/mL (%)	200 μg/mL (%)	300 μg/mL (%)	500 μg/mL (%)
MC-1	0.18 ± 0.32	0.36 ± 0.29	0.79 ± 0.35	0.71 ± 0.24
MC-2	0.13 ± 0.04	0.33 ± 0.12	0.43 ± 0.12	0.63 ± 0.04
MC-3	0.25 ± 0.04	0.15 ± 0.20	0.30 ± 0.27	0.76 ± 0.66

[a]Standard deviation is calculated from three samples.

strong function of porosity, shape, and size.[47−49] Comparison of hemolysis data with mesoporous silica suggests that silica can cause hemolysis as high as 20−80%[47,48] at the highest concentration of the study (500 μg/mL); these results are orders of magnitude higher than our results. Although the mesoporous carbon employed in our study was not nanosized and it may appear that the size effect was not investigated, Zhao et al.[49] confirmed that the smaller particles, in fact, can potentially be safe toward RBC as they get adsorbed onto the RBC surface without disturbing the cell membrane or morphology. Based on this finding, we can draw a hypothesis that nanosized mesoporous carbon may possess an even lesser threat toward intravascular drug delivery. This suggests that mesoporous carbon material can serve as a better choice over mesoporous silica for intravascular drug delivery.

The amount of plasma protein adsorption onto biomaterials is an important parameter toward its biocompatibility in terms of implants, intravascular delivery and tissue engineering. When a foreign body comes in contact with the bloodstream, the surface could be rapidly covered with plasma protein, often termed the protein corona.[50,51] Although in rare occasions where fibronectin adsorption has facilitated cell attachment,[52,53] nonspecific adsorption of proteins onto the biomaterial surface is mostly undesirable as it may trigger adverse effects, such as localized inflammation, hyperactive immune response, or conformational changes of protein structure leading to loss of activity[54] and thrombolysis.[55,56] Here, we have studied the nonspecific adsorption of two plasma proteins: bovine serum

albumin (BSA) and bovine serum fibrinogen (FIB). Table 4 shows the results of protein adsorption.

Table 4. Protein Adsorption on Mesoporous Carbon Samples[a]

carbon species	BSA adsorption, (g of protein/m^2 of carbon) × 10^{-4}	FIB adsorption, (g of protein/m^2 of carbon) × 10^{-4}
MC-1	2.21 ± 0.31	25.5 ± 3.48
MC-2	3.01 ± 0.03	38.1 ± 0.93
MC-3	6.08 ± 1.72	48.8 ± 1.82

[a]Standard deviation is calculated from three samples.

As BET SSA encompasses a large portion of narrow micropore surfaces that may not take part in larger protein adsorption, we employed external SSA (Table 2) for calculating protein-binding capacity. We found that BSA adsorption was <1 mg/m^2 of carbon surface, whereas fibrinogen adsorption was 1 order of magnitude higher, 2−4 mg/m^2.

The BSA adsorption capacity was in line with the overall protein adsorption onto other porous biomaterials, like hydroxyapatite, zirconia, and alumina.[55] A comparison of BSA adsorption on mesoporous carbon samples (1−2 nmol protein/mg carbon) with human serum albumin (HSA) adsorption onto mesoporous silica nanoparticles (MSN;[56] 3−7 nmol protein/mg MSN) suggests that the carbon surface provides less affinity toward albumin. Although fibrinogen adsorption was higher (more than 3 nmol protein/mg carbon), we could not compare its adsorption with other porous biomaterials owing to the lack of reported data. Slightly higher affinity toward fibrinogen may result in somewhat higher risk of thrombolysis, but as suggested in the literature, functionalization or covering the surface with biocompatible PEG molecules will reduce such risk.[57]

To estimate the percent monolayer coverage, we employed a closed packing hard-sphere model of adsorbed proteins. The monolayer model suggests a surface density of 4.8 and 8.5 mg/m^2 for BSA and FIB, respectively. On the basis of these surface densities, we estimated that BSA covered 4.5, 6.1, and 12.4% of MC-1, MC-2, and MC-3, respectively, whereas FIB possesses the higher surface coverage of 26.5, 43.2, and 57.9% for MC-1, MC-2, and MC-3, respectively. Although the ideal hard sphere model can be deviated in terms of (1) uncoiling or flattening of the protein molecule in proximity to adsorption surfaces[58,59] and (2) nonspecific and undesirable locations of calculated external surfaced area, the coverage percent can provide an approximation of surface occupancies by protein molecules.

A clear pattern of protein adsorption onto mesoporous carbons can be deduced. For both types of proteins, the adsorption capacity increases in the order of MC-1 < MC-2 < MC-3. It is observed that fibrinogen adsorption is 1 order of magnitude higher for all three types of carbons. Although the higher protein adsorption to MC-2 and MC-3 can be related to the higher oxygen content resulting in a greater number of hydrogen bonds, such an explanation does not fully support the trend in loading amounts. The explanations for higher fibrinogen binding and patterned relation between binding capacity and materials properties definitely require much more detailed research and understanding of carbon surface, including precise functionality characterization, hydrophobicity/hydrophilicity, and Z-potential determination ,which are beyond the scope of this work. Nonetheless, the protein adsorption data suggest that the carbon surface is mostly biocompatible and similar to the other biomaterials.

4. CONCLUSIONS

In this work, we have studied the in vitro biocompatibility of soft-templated mesoporous carbons by cytotoxicity experiments with HeLa cells, cell viability with fibroblast cells and blood compatibility with hemolysis and protein adsorption. MC-2 and MC-3 samples showed minimal cytotoxicity while MC-1 demonstrated only slight toxicity within the concentrations of 50−500 μg/mL. Cell growth assays with fibroblast cells demonstrated a constant viability at a concentration of 100 μg/mL of mesoporous carbons and a clear visual observation of cell-carbon contact was confirmed. None of the carbon samples demonstrated hemolysis (<1%). Protein adsorption with bovine serum albumin (BSA) and fibrinogen demonstrated lower protein binding with a decreasing trend with an increase in carbon surface area. All the results suggested that the mesoporous carbon materials are biocompatible, and the degree of biocompatibility is within the range or higher than other biomaterials currently employed in biomedical applications.

AUTHOR INFORMATION

Corresponding Authors

*E-mail: heldt@mtu.edu.

*E-mail: dsaha@mail.widener.edu, dipendus@gmail.com. Tel: 610 499 4056. Fax: 610 499 4059.

Notes

The authors declare no competing financial interest.

ACKNOWLEDGMENTS

The authors would like to thank K. Saagar Vijayaragavan and Owen Mills for assistance with the FE-SEM images of cells on the mesoporous carbon structures, and Adrienne Minerick for providing blood samples. TEM, EDXS, and SEM analyses were conducted at the Center for Nanophase Materials Sciences, which is sponsored at Oak Ridge National Laboratory by the Division of Scientific User Facilities, Office of Basic Energy Sciences, U.S. Department of Energy. M.F.G. and C.L.H thank the Department of Chemical Engineering at Michigan Technological University for funding. D.S. acknowledges the start-up grant and faculty development award from the School of Engineering at Widener University.

REFERENCES

(1) Rammohan, A.; Tayal, L.; Kumar, A.; Sivakumar, S.; Sharma, A. Fabrication of Polymer-Modified Monodisperse Mesoporous Carbon Particles by Template-Based Approach for Drug Delivery. *RSC Adv.* **2013**, *3*, 2008−2016.

(2) Smart, S.; Cassady, A.; Lu, G.; Martin, D. The Biocompatibility of Carbon Nanotubes. *Carbon* **2006**, *44*, 1034−1047.

(3) Warheit, D. What Is Currently Known About the Health Risks Related to Carbon Nanotube Exposures? *Carbon* **2006**, *44*, 1064−1069.

(4) Hurt, R. H.; Monthioux, M.; Kane, A. Toxicology of Carbon Nanomaterials: Status, Trends, and Perspectives on the Special Issue. *Carbon* **2006**, *44*, 1028−1033.

(5) Murray, A.; Kisin, E.; Leonard, S.; Young, S.; Kommineni, C.; Kagan, V.; Castranova, V.; Shvedova, A. Oxidative Stress and Inflammatory Response in Dermal Toxicity of Single-Walled Carbon Nanotubes. *Toxicology* **2009**, *257*, 161−171.

(6) Muller, J.; Huaux, F.; Moreau, N.; Misson, P.; Heilier, J.-F.; Delos, M.; Arras, M.; Fonseca, A.; Nagy, J. B.; Lison, D. Respiratory

Toxicity of Multi-Wall Carbon Nanotubes. *Toxicol. Appl. Pharmacol.* **2005**, *207*, 221−231.
(7) Muller, J.; Huaux, F.; Lison, D. Respiratory Toxicity of Carbon Nanotubes: How Worried Should We Be? *Carbon* **2006**, *44*, 1048−1056.
(8) Inoue, K.-I.; Yanagisawa, R.; Koike, E.; Nishikawa, M.; Takano, H. Repeated Pulmonary Exposure to Single-Walled Carbon Nanotubes Exacerbates Allergic Inflammation of the Airway: Possible Role of Oxidative Stress. *Free Radical Biol. Med.* **2010**, *48*, 924−934.
(9) Kayat, J.; Gajbhiye, V.; Tekade, R. K.; Jain, N. K. Pulmonary Toxicity of Carbon Nanotubes: A Systematic Report. *Nanomedicine* **2011**, *7*, 40−49.
(10) Wick, P.; Manser, P.; Limbach, L. K.; Dettlaff-Weglikowska, U.; Krumeich, F.; Roth, S.; Stark, W. J.; Bruininck, A. The Degree and Kind of Agglomeration Affect Carbon Nanotube Cytotoxicity. *Toxicol. Lett.* **2007**, *168*, 121−131.
(11) Zhu, S.; Oberdörster, E.; Haasch, M. L. Toxicity of an Engineered Nanoparticle (Fullerene, C60) in Two Aquatic Species, *Daphnia* and Fathead Minnow. *Mar. Environ. Res.* **2006**, *62*, S5−S9.
(12) Cui, F.; Li, D. A Review of Investigations on Biocompatibility of Diamond-Like Carbon and Carbon Nitride Films. *Surf. Coat. Technol.* **2000**, *131*, 481−487.
(13) Grill, A. Diamond-Like Carbon Coatings as Biocompatible Materials—An Overview. *Diamond Relat. Mater.* **2003**, *12*, 166−170.
(14) Hauert, R. A Review of Modified DLC Coatings for Biological Applications. *Diamond Relat. Mater.* **2003**, *12*, 583−589.
(15) Corby, D. G.; Decker, W. J. Management of Acute Poisoning with Activated Charcoal. *Pediatrics* **1974**, *54*, 324−329.
(16) Chyka, P.; Seger, D. Position Statement: Single-Dose Activated Charcoal. American Academy of Clinical Toxicology; European Association of Poisons Centres and Clinical Toxicologists. *J. Toxicol., Clin. Toxicol.* **1996**, *35*, 721−741.
(17) Warheit, D. B.; Sayes, C. M.; Reed, K. L.; Swain, K. A. Health Effects Related to Nanoparticle Exposures: Environmental, Health, and Safety Considerations for Assessing Hazards and Risks. *Pharmacol. Ther.* **2008**, *120*, 35−42.
(18) Saha, D.; Payzant, E. A.; Kumbhar, A. S.; Naskar, A. K. Sustainable Mesoporous Carbons as Storage and Controlled-Delivery Media for Functional Molecules. *ACS Appl. Mater. Interfaces* **2013**, *5*, 5868−5874.
(19) Saha, D.; Warren, K. E.; Naskar, A. K. Soft-Templated Mesoporous Carbons as Potential Materials for Oral Drug Delivery. *Carbon* **2014**, *71*, 47−57.
(20) Saha, D.; Warren, K. E.; Naskar, A. K. Controlled Release of Antipyrine from Mesoporous Carbons. *Microporous Mesoporous Mater.* **2014**, *196*, 327−334.
(21) Wang, X.; Liu, P.; Tian, Y.; Zang, L. Novel Synthesis of Fe-Containing Mesoporous Carbons and Their Release of Ibuprofen. *Microporous Mesoporous Mater.* **2011**, *145*, 98−103.
(22) Karavasili, C.; Amanatiadou, E. P.; Sygellou, L.; Giasafaki, D. K.; Steriotis, T. A.; Charalambopoulou, G. C.; Vizirianakis, I. S.; Fatouros, D. G. Development of New Drug Delivery System Based on Ordered Mesoporous Carbons: Characterisation and Cytocompatibility Studies. *J. Mater. Chem. B* **2013**, *1*, 3167−3174.
(23) Zhao, P.; Wang, L.; Sun, C.; Jiang, T.; Zhang, J.; Zhang, Q.; Sun, J.; Deng, Y.; Wang, S. Uniform Mesoporous Carbon as a Carrier for Poorly Water Soluble Drug and Its Cytotoxicity Study. *Eur. J. Pharm. Biopharm.* **2012**, *80*, 535−543.
(24) Zhu, J.; Liao, L.; Bian, X.; Kong, J.; Yang, P.; Liu, B. pH-Controlled Delivery of Doxorubicin to Cancer Cells, Based on Small Mesoporous Carbon Nanospheres. *Small* **2012**, *8*, 2715−2720.
(25) Gu, J.; Su, S.; Li, Y.; He, Q.; Shi, J. Hydrophilic Mesoporous Carbon Nanoparticles as Carriers for Sustained Release of Hydrophobic Anti-Cancer Drugs. *Chem. Commun.* **2011**, *47*, 2101−2103.
(26) Labiano, A.; Dai, M.; Taylor, D.; Young, W.-S.; Epps, T. H., III; Rege, K.; Vogt, B. D. Slow Release Kinetics of Mitoxantrone from Ordered Mesoporous Carbon Films. *Microporous Mesoporous Mater.* **2012**, *160*, 143−150.
(27) Kortesuo, P.; Ahola, M.; Karlsson, S.; Kangasniemi, I.; Yli-Urpo, A.; Kiesvaara, J. Silica Xerogel as an Implantable Carrier for Controlled Drug Delivery—Evaluation of Drug Distribution and Tissue Effects after Implantation. *Biomaterials* **2000**, *21*, 193−198.
(28) Burns, C.; Zarkower, A.; Ferguson, F. Murine Immunological and Histological Changes in Response to Chronic Silica Exposure. *Environ. Res.* **1980**, *21*, 298−307.
(29) Allison, A.; Harington, J.; Birbeck, M. An Examination of the Cytotoxic Effects of Silica on Macrophages. *J. Exp. Biol.* **1966**, *124*, 141−154.
(30) Gopinath, C.; Prentice, D. E.; Lewis, D. J. *Atlas of Experimental Toxicological Pathology*. MTP Press: Lancaster, U.K., 1987.
(31) Vinu, A.; Miyahara, M.; Ariga, K. Preparation and Pore Size Control of Cage Type Mesoporous Carbon Materials and Their Application in Protein Adsorption. *Stud. Surf. Sci. Catal.* **2005**, *158*, 971−978.
(32) Kim, T.-W.; Chung, P.-W.; Slowing, I. I.; Tsunoda, M.; Yeung, E. S.; Lin, V. S.-Y. Structurally Ordered Mesoporous Carbon Nanoparticles as Transmembrane Delivery Vehicle in Human Cancer Cells. *Nano Lett.* **2008**, *8*, 3724−3727.
(33) Fang, Y.; Gu, D.; Zou, Y.; Wu, Z.; Li, F.; Che, R.; Deng, Y.; Tu, B.; Zhao, D. A Low-Concentration Hydrothermal Synthesis of Biocompatible Ordered Mesoporous Carbon Nanospheres with Tunable and Uniform Size. *Angew. Chem., Int. Ed.* **2010**, *49*, 7987−7991.
(34) Tafur, M. F.; Vijayaragavan, K. S.; Heldt, C. L. Reduction of Porcine Parvovirus Infectivity in the Presence of Protecting Osmolytes. *Antiviral Res.* **2013**, *99*, 27−33.
(35) Fan, H.; Liu, G.; Huang, Y.; Li, Y.; Xia, Q. Development of a Nanostructured Lipid Carrier Formulation for Increasing Photo-Stability and Water Solubility of Phenylethyl Resorcinol. *Appl. Surf. Sci.* **2014**, *288*, 193−200.
(36) Correa-Duarte, M. A.; Wagner, N.; Rojas-Chapana, J.; Morsczeck, C.; Thie, M.; Giersig, M. Fabrication and Biocompatibility of Carbon Nanotube-Based 3D Networks as Scaffolds for Cell Seeding and Growth. *Nano Lett.* **2004**, *4*, 2233−2236.
(37) Abarrategi, A.; Gutierrez, M. C.; Moreno-Vicente, C.; Hortigüela, M. J.; Ramos, V.; Lopez-Lacomba, J. L.; Ferrer, M. L.; del Monte, F. Multiwall Carbon Nanotube Scaffolds for Tissue Engineering Purposes. *Biomaterials* **2008**, *29*, 94−102.
(38) Cui, D.; Tian, F.; Ozkan, C. S.; Wang, M.; Gao, H. Effect of Single Wall Carbon Nanotubes on Human HEK293 Cells. *Toxicol. Lett.* **2005**, *155*, 73−85.
(39) Di Pasqua, A. J.; Sharma, K. K.; Shi, Y.-L.; Toms, B. B.; Ouellette, W.; Dabrowiak, J. C.; Asefa, T. Cytotoxicity of Mesoporous Silica Nanomaterials. *J. Inorg. Biochem.* **2008**, *102*, 1416−1423.
(40) Heikkilä, T.; Santos, H. A.; Kumar, N.; Murzin, D. Y.; Salonen, J.; Laaksonen, T.; Peltonen, L.; Hirvonen, J.; Lehto, V.-P. Cytotoxicity Study of Ordered Mesoporous Silica MCM-41 and SBA-15 Microparticles on Caco-2 Cells. *Eur. J. Pharm. Biopharm.* **2010**, *74*, 483−494.
(41) Kasemo, B. Biological Surface Science. *Surf. Sci.* **2002**, *500*, 656−677.
(42) Santos, H. A.; Riikonen, J.; Salonen, J.; Mäkilä, E.; Heikkilä, T.; Laaksonen, T.; Peltonen, L.; Lehto, V.-P.; Hirvonen, J. In Vitro Cytotoxicity of Porous Silicon Microparticles: Effect of the Particle Concentration, Surface Chemistry and Size. *Acta Biomater.* **2010**, *6*, 2721−2731.
(43) Chang, E.-J.; Kim, H.-H.; Huh, J.-E.; Kim, I.-A.; Ko, J. S.; Chung, C.-P.; Kim, H.-M. Low Proliferation and High Apoptosis of Osteoblastic Cells on Hydrophobic Surface Are Associated with Defective Ras Signaling. *Exp. Cell Res.* **2005**, *303*, 197−206.
(44) Mitragotri, S.; Lahann, J. Physical Approaches to Biomaterial Design. *Nat. Mater.* **2009**, *8*, 15−23.
(45) Fujii, M.; Nishimura, N.; Fumon, H.; Hayashi, S.; Kovalev, D.; Goller, B.; Diener, J. Dynamics of Photosensitized Formation of Singlet Oxygen by Porous Silicon in Aqueous Solution. *J. Appl. Phys.* **2006**, *100*, 124302.
(46) Allen, M.; Myer, B.; Rushton, N. In Vitro and in Vivo Investigations into the Biocompatibility of Diamond-Like Carbon

(DLC) Coatings for Orthopedic Applications. *J. Biomed. Mater. Res.* **2001**, *58*, 319−328.
(47) Lin, Y.-S.; Haynes, C. L. Impacts of Mesoporous Silica Nanoparticle Size, Pore Ordering, and Pore Integrity on Hemolytic Activity. *J. Am. Chem. Soc.* **2010**, *132*, 4834−4842.
(48) Yu, T.; Malugin, A.; Ghandehari, H. Impact of Silica Nanoparticle Design on Cellular Toxicity and Hemolytic Activity. *ACS Nano* **2011**, *5*, 5717−5728.
(49) Zhao, Y.; Sun, X.; Zhang, G.; Trewyn, B. G.; Slowing, I. I.; Lin, V. S.-Y. Interaction of Mesoporous Silica Nanoparticles with Human Red Blood Cell Membranes: Size and Surface Effects. *ACS Nano* **2011**, *5*, 1366−1375.
(50) Lundqvist, M.; Stigler, J.; Cedervall, T.; Berggård, T.; Flanagan, M. B.; Lynch, I.; Elia, G.; Dawson, K. The Evolution of the Protein Corona around Nanoparticles: A Test Study. *ACS Nano* **2011**, *5*, 7503−7509.
(51) Casals, E.; Pfaller, T.; Duschl, A.; Oostingh, G. J.; Puntes, V. Time Evolution of the Nanoparticle Protein Corona. *ACS Nano* **2010**, *4*, 3623−3632.
(52) Horbett, T. A. The Role of Adsorbed Proteins in Animal Cell Adhesion. *Colloids Surf., B* **1994**, *2*, 225−240.
(53) Ducheyne, P.; Qiu, Q. Bioactive Ceramics: The Effect of Surface Reactivity on Bone Formation and Bone Cell Function. *Biomaterials* **1999**, *20*, 2287−2303.
(54) Grinnell, F.; Feld, M. K. Adsorption Characteristics of Plasma Fibronectin in Relationship to Biological Activity. *J. Biomed. Mater. Res.* **1981**, *15*, 363−381.
(55) Rosengren, Å.; Pavlovic, E.; Oscarsson, S.; Krajewski, A.; Ravaglioli, A.; Piancastelli, A. Plasma Protein Adsorption Pattern on Characterized Ceramic Biomaterials. *Biomaterials* **2002**, *23*, 1237−1247.
(56) Yildirim, A.; Ozgur, E.; Bayindir, M. Impact of Mesoporous Silica Nanoparticle Surface Functionality on Hemolytic Activity, Thrombogenicity, and Non-Specific Protein Adsorption. *J. Mater. Chem. B* **2013**, *1*, 1909−1920.
(57) He, Q.; Zhang, J.; Shi, J.; Zhu, Z.; Zhang, L.; Bu, W.; Guo, L.; Chen, Y. The Effect of Pegylation of Mesoporous Silica Nanoparticles on Nonspecific Binding of Serum Proteins and Cellular Responses. *Biomaterials* **2010**, *31*, 1085−1092.
(58) Horbett, T. A. *Biomaterials: Interfacial Phenomena and Applications*. Cooper, S. L.; Peppas, N. A.; Hoffman, A. S.; Ratner, B. D., Eds. American Chemical Society: Washington, D.C., 1982; Chapter 17, pp 233−244.
(59) Norde, W.; MacRitchie, F.; Nowicka, G.; Lyklema, J. Protein Adsorption at Solid−Liquid Interfaces: Reversibility and Conformation Aspects. *J. Colloid Interface Sci.* **1986**, *112*, 447−456.